The impact of reaction conditions and material composition on the stepwise methane to methanol conversion over Cu-MOR: An *operando* XAS study

K.A. Lomachenko[a], A. Martini[b,c], D.K. Pappas[d], C. Negri[e], M. Dyballa[d], G. Berlier[e], S. Bordiga[d,e], C. Lamberti[b,c], U. Olsbye[d], S. Svelle[d], P. Beato[f], E. Borfecchia[e,f,*]

[a] European Synchrotron Radiation Facility, 71 Avenue des Martyrs, CS 40220, 38043 Grenoble Cedex 9, France
[b] Department of Physics, NIS Interdepartmental Center and INSTM Reference Center, University of Turin, Via P. Giuria 1, 10125 Turin, Italy
[c] The Smart Materials Research Institute, Southern Federal University, Sladkova Street 174/28, 344090 Rostov-on-Don, Russia
[d] Center for Materials Science and Nanotechnology (SMN), Department of Chemistry, University of Oslo, 1033 Blindern, 0315 Oslo, Norway
[e] Department of Chemistry, NIS Interdepartmental Center and INSTM Reference Center, University of Turin, Via P. Giuria 7, 10125 Turin, Italy
[f] Haldor Topsøe A/S, Haldor Topsøes Allé 1, 2800 Kongens Lyngby, Denmark

ARTICLE INFO

ABSTRACT

The direct methane to methanol (DMTM) conversion is often referred to as a 'dream reaction' with enormous potential to alter energy sector and chemical industry. After O_2-activation, Cu-exchanged zeolites form Cu_xO_y species that activate CH_4 and release it in the form of CH_3OH upon interaction with H_2O. Despite extensive research efforts in the last years, several questions concerning the influence of materials composition and process parameters on the reaction mechanism remain open. Herein, we characterize Cu-MOR zeolites with different composition by *operando* X-ray absorption spectroscopy (XAS), monitoring their spectroscopic response under two characteristic DMTM reaction protocols varied in the duration of the key reaction steps. Linear Combination Fit (LCF) analysis of the time-resolved X-ray absorption near edge structure (XANES) spectra collected during CH_4-loading and steam-assisted CH_3OH extraction enabled to quantify the abundance of different Cu species during these two steps. Data analysis revealed a positive linear correlation between the methanol yield generated per incorporated copper and the Cu(I) component formed during the CH_4-loading step. Cu(I) development during CH_4-loading is accompanied by modifications in the extended X-ray absorption fine structure (EXAFS) spectra suggesting substantial rearrangement in the active site structure. The obtained results provide new mechanistic insights for the DMTM over Cu-MOR.

1. Introduction

Methane (CH_4) constitutes the major component of natural gas and is largely utilized as an energy carrier and basis for chemicals production [1]. However, due to transportation challenges huge amounts of CH_4 are flared and vented, contributing to the greenhouse effect and resulting in the sheer waste of an abundant natural resource [2]. Current industrial processes for the conversion of CH_4 to liquid chemicals, especially oxygenates such as CH_3OH, - pass through the syngas route. The latter process requires the highly energy-intensive production of synthesis gas (mixture of CO, H_2 and CO_2) prior to methanol synthesis, hindering its implementation for small-scale use, due to the so-called rule of 'economy of scale' [3]. Therefore, the direct conversion of CH_4 to oxygenates has been investigated for several decades and even applied industrially, especially in the first half of the 20th century in the United

States [4], due to the large economic and environmental benefits that it could provide [5–8]. However, a direct process with high conversion and selectivity to high-value products is far from commercial realization.

The direct selective oxidation of CH_4 to CH_3OH over Cu-zeolites has been first reported by Groothaert et al. for the MFI framework [9] and thoroughly studied by different research groups in the recent years, extending the scope to other framework structures [10–14]. The conversion is achieved through a chemical looping approach. The zeolite is initially activated in oxidizing atmosphere (commonly in O_2) at high temperature (400–500 °C) in order to generate active Cu_xO_y moieties. These species then are able to activate CH_4 and stabilize the reaction intermediates at lower temperatures, typically 200 °C. These are subsequently isothermally extracted by hydrolysis with water vapour in the form of oxygenates *i.e.* CH_3OH and CH_3OCH_3. Recently, the conversion

was also demonstrated under anaerobic conditions. In such a process scheme, the H_2O molecules used for extraction are proposed to play a twofold role: they energetically favor CH_3OH desorption and regenerate the active Cu site through water splitting under H_2 generation [13,15].

For both approaches, different Cu-exchanged zeolite structures have been proved to be active, among them Cu-MOR [11,13,16,17], Cu-MAZ [18,19], and Cu-CHA [12,20–22] exhibiting highest yields. The exact nature and structure of active sites responsible for the DMTM reaction is still debated and a variety of Cu-oxo species have been suggested to possess such activity, mostly defined by the zeolite topology. Specifically, for Cu-MOR the differences in Cu/Al ratio, the origin of the parent material, the copper exchange procedure and the activation conditions result in Cu-oxo species with different nuclearity hosted at extra-framework sites in the zeolite. Mono-, di- and tri-copper configurations have been proposed as possible active sites, with different stability and activity [11,13,15,23,24].

Sushkevich et al. observed that rising Si/Al ratio of the MOR framework decreases the nuclearity of the Cu sites formed in the pores, with low Al contents enhancing the population of mono-copper species [15]. In the same context, we have recently applied multivariate curve resolution (MCR) analysis of high-energy resolution X-ray Absorption Spectroscopy (XAS) data to discriminate among active and inactive Cu in O_2-activated MOR materials with different composition. Data analysis unambiguously revealed di-copper Cu_2O_x active site in the investigated sample series [16].

Overall, correlation of the material properties with productivity data as well as spectroscopic results point to the coexistence of multiple active and inactive Cu configurations. Apart from the different nature of active sites towards activation of CH_4, the reaction conditions have been identified to affect the productivity of the Cu-zeolite [12,16,18,25]. Prolonged O_2 activation at high temperature, long reaction times with CH_4, and reaction with CH_4 at high pressure have all shown to boost the productivity [8,12,18,26]

Following the generation of Cu active species during high-temperature treatment in oxidizing atmosphere, CH_4 is introduced and oxidized. The cleavage of the C-H bond has been early proposed as the rate limiting step by Woertink et al. [27]. Later findings through density functional theory (DFT) modelling suggested that the activation of CH_4 requires two adjacent mono(μ-oxo)dicopper sites able to host the methyl radical as well as the free proton resulting into [Cu(I)-OCH$_3$-Cu(II)] and [Cu(I)-OH-Cu(II)] as reaction intermediates [28]. This mechanism implies that four copper atoms in two di-copper sites participate in forming one CH_3OH molecule. This limits the maximum allowed stoichiometric productivity to 0.25 mol CH_3OH/mol Cu, while half of the Cu is reduced from Cu(II) to Cu(I). Recently Sushkevich et al. [13] evidenced by FTIR an increased Brønsted acidity during the activation of CH_4, accompanied by the rise of a band corresponding to methoxy species. Based on these spectroscopic evidences, the authors proposed that a single CH_4 molecule is activated on a di-copper site resulting in a methoxy group stabilized at the Cu active site and one Brønsted site formed in its proximity [13]. The reduction of Cu(II) to Cu(I) has been a well-evidenced phenomenon during CH_4-loading over O_2-activated Cu-MOR zeolites [11,13,21,28–30], corroborating the proposed mechanisms.

Herein, we study two Cu-MOR zeolites by *operando* XAS, monitoring their spectroscopic properties during application of two characteristic DMTM reaction protocols. We investigate thereby the need for and effects of increasing duration of key reaction steps, directly comparing the Cu K-edge XAS of Cu-MOR for selected combinations of sample composition and process protocols. The collected datasets show significant differences, mostly evident during the CH_4-loading and steam-assisted CH_3OH-extraction step. We show how the Cu-speciation can be quantified by applying LCF analysis to the time-dependent XANES collected during these steps, and how it can be linked to the performance of the materials under different protocols. Through these correlations, XANES LCF results in combination with EXAFS and on-line

MS provide novel insights in the DMTM reaction mechanism over Cu-MOR.

2. Materials and methods

2.1. Synthesis and physico-chemical characterization

Commercial zeolites from Zeolyst were used as starting materials: CBV21A (NH$_4$-MOR, Si/Al = 11) and CBV10ADS (Na-MOR, Si/Al = 7). Both were ion-exchanged with NH$_4$NO$_3$ (10 wt% in water) at 60 °C for 5 h, one and three times respectively. Then the samples were washed NO$_3$-free and NH$_3$ was burned off by heating (1 °C/min) in air at 500 °C for 8 h. The resulting H-form zeolites were cooled to RT, slowly rehydrating in air and then exchanged. Aqueous solutions of copper acetate (99.99%, Sigma-Aldrich) with 0.01 and 0.02 M were used for the exchange with a ratio of 60 mL$_{solution}$/g$_{zeolite}$. The process was conducted overnight under stirring at RT while adjusting the pH between 5.2 and 5.7 using a NH$_4$OH-solution (28%, Sigma-Aldrich). After exchange, the materials were washed three times with water in order to remove excess copper ions and avoid overloading.

The dispersion of Cu ions as well as the absence of large aggregates were confirmed by Scanning Electron Microscopy (SEM) and X-Ray Diffraction (XRD). The compositional characteristics of the two Cu-MOR samples, determined by Energy Dispersive X-Ray Spectroscopy (EDS), are summarized in Table 1. In the following, the two materials will be identified as xCu-HMOR(y), where x = Cu/Al and y = Si/Al ratios.

2.2. Operando X-ray absorption spectroscopy (XAS)

Operando XAS data during the DMTM conversion over 0.18Cu-HMOR(7) and 0.36Cu-HMOR(11) were collected at the BM31 [31] and BM23 [32] beamlines of the European Synchrotron Radiation Facility (ESRF, Grenoble, France).

At the BM31 beamline the stepwise reaction was carried out according to the 'Short Protocol' (SP) schemed in Fig. 1a. The experiments were conducted by loading ca. 3 mg of powder in a 1 mm diameter capillary reactor connected to an appropriate gas-flow setup. Temperature at the data collection point was controlled by a heat gun. A heating/cooling rate of 5 °C/min and a total flow rate of 2 ml/min were employed for all the steps of the SP, namely O_2-activation at 500 °C (90 min, 100% O_2), CH_4-loading at 200 °C (120 min, 100% CH_4), and steam-assisted CH_3OH extraction at 200 °C (ca. 60 min). Extraction was performed by flowing a 10% Ar/He mixture through a saturator with deionized water at 44 °C. The steam was then introduced to the sample and the effluent was analysed by a quadrupole mass spectrometer (MS), from Pfeiffer Vacuum. Using a capillary reactor (no dead volume, conveniently approximating a fixed-bed reactor), it was possible to quantify the CH_3OH yield per Cu on-line during the *operando* XAS experiments (see Fig. 7b,c, bottom panels).

Cu K-edge XAS spectra were collected in transmission mode, using a water-cooled flat Si(111) double-crystal monochromator detuned down to 65% of the maximum intensity for harmonics rejection. The incident (I$_0$) and transmitted (I$_1$) X-ray intensity were detected using 30 cm ionization chambers filled with a mixture of He and Ar. Continuous scans (with a constant angular speed of the monochromator) were performed in the 8800–9300 eV range with a 0.5 eV sampling. Acquisition time

Table 1
Identification and compositional characteristics of the investigated Cu-MOR samples, determined by EDS.

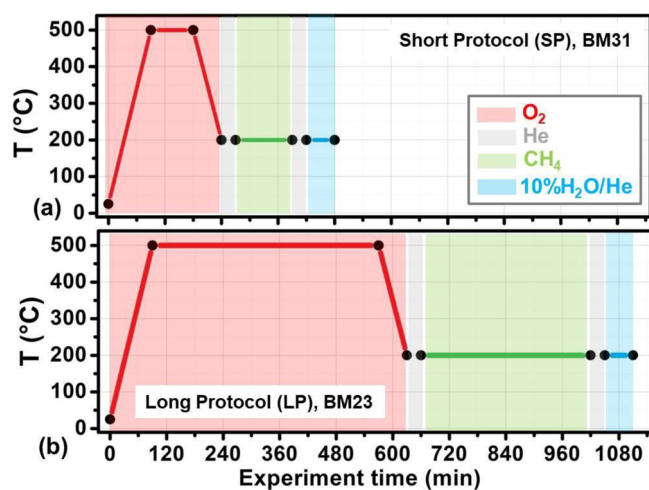| Sample	Si/Al	Cu/Al	Cu wt%
0.36Cu-MOR(11)	11	0.36	3.18
0.18Cu-HMOR(7)	7	0.18	2.33

Fig. 1. Schematic representation of the protocols adopted to monitor by *operando* XAS the stepwise DMTM conversion over Cu-MOR at (a) the BM31 beamline (Short Protocol, SP) and (b) at the BM23 beamline (Long Protocol, LP).

was ca. 5 min/scan. At the end of each reaction step along the SP, two longer scans (ca. 10 min/scan) were acquired, in the 8800–10000 eV range.

At the BM23 beamline, the DMTM reaction was carried out according to the 'Long Protocol' (LP), schemed in Fig. 1b. Aiming to get higher data quality in the EXAFS region, here we measured the same two Cu-MOR materials in the form of self-supporting pellets (optimized samples weights in the 100–110 mg range for 1.3 cm^2 area pellets, resulting in edge jumps $\Delta\mu x$ in the $0.4-0.6$ range for a total absorption after the edge of $\mu x = 2.5$). The pelletized Cu-zeolites were hosted in an *ad hoc* reactor cell developed at the BM23/ID24 beamlines of the ESRF [33]. After fixing the sample pellet inside, the reactor cell was closed and connected to a dedicated gas flow setup for the DMTM reaction. A heating/cooling rate of 5 °C/min and a total flow rate of 8 ml/min was employed for all the steps of the LP, including O_2-activation at 500 °C (480 min, 100% O_2), CH_4-loading at 200 °C (360 min, 100% CH_4), and steam-assisted CH_3OH extraction at 200 °C (ca. 60 min). Extraction was performed by flowing Ar/He through a saturator with deionized water at 44 °C. The steam was then sent to the sample and the effluent was monitored by MS, as shown in Fig. 2. With this experimental setup, MS allowed to qualitatively verify presence of the reaction products. However, due to the not negligible dead volume of the cell along with the small quantities of extracted product, it was not possible to use these collected MS data for quantification of the products.

Cu K-edge XAS spectra for the LP were collected at BM23 in transmission mode, using a LN_2-cooled flat Si(111) double-crystal monochromator. The incident (I_0) and transmitted ($I_{1,2}$) X-ray intensities were detected using ionization chambers filled with a mixture of He and Ar. The third ionization chamber (I_2) was used for the simultaneous collection of the XANES spectrum of a Cu metal foil for the energy calibration of each spectrum [34]. Rejection of higher harmonics was done by two flat Si mirrors positioned at the angle of 2.5 mrad with respect to the incident beam. XAS scans were acquired in the 8800–9727 eV range, with the energy step of 5 eV in the pre-edge region, 0.2 eV in the XANES region and a constant k step of $\Delta k = 0.035$ Å^{-1} in the EXAFS region. Integration time was 1 s/point, resulting in ca. 15 min/scan.

The XAS spectra collected at both beamlines were normalized to unity edge jump using the Athena software from the Demeter package [35]. $\chi(k)$ EXAFS functions were also extracted by using the Athena program. For the scans collected on the BM23 beamline, Fourier-transform (FT) EXAFS spectra were obtained by transforming the $k^2\chi(k)$ functions in the (2.4–11.0) Å^{-1} range, thanks to the higher data
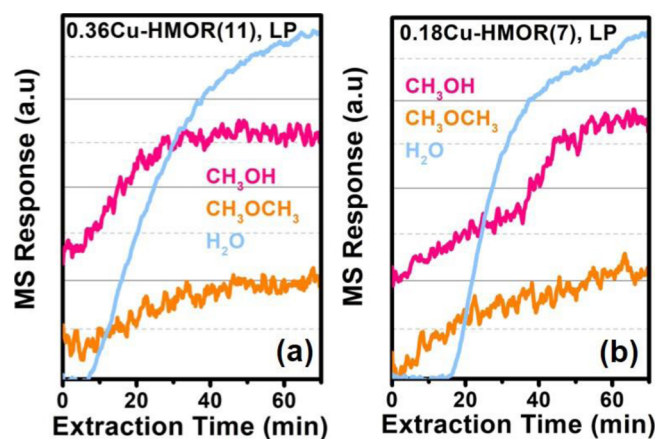
quality achieved by using a pelletized sample. For the two longer scans collected on BM31 at the end of each reaction step, consistently with the lower homogeneity of powdered samples in a capillary reactor, a shorter (2.4–8.7) Å^{-1} k-range was used for the FT.

2.3. XAS linear combination fit (LCF) analysis

Linear combination fit (LCF) analysis of the time-dependent *operando* XANES μ^{exp} (E) was performed in the 8970–9020 eV energy interval, using the Athena software from the Demeter package [35]. The *operando* XANES spectra collected during CH_4-loading and steam-assisted CH_3OH extraction were analysed using the three reference spectra shown in Fig. 5a. These are representative of pseudo-octahedral Cu(II) aquo complexes (*Cu(II)-hyd*) as well as framework-coordinated Cu(II) and Cu(I) species, referred to as *Cu(II)-MOR* and *Cu(I)-MOR*, respectively. *Cu(II)-hyd* was obtained by measuring a Cu(II) acetate aqueous solution at RT. *Cu(I)-MOR* was obtained by heating at 400 °C in vacuum the 0.36Cu-HMOR(11) material and by cooling the sample to RT after the thermal treatment while keeping it under vacuum for the XAS measurements in an *ad hoc* cell. *Cu(II)-MOR* is the XANES collected for each experiment in He at 200 °C after O_2-activation at 500 °C. This step is representative to the Cu(II) species just before the CH_4-loading step.
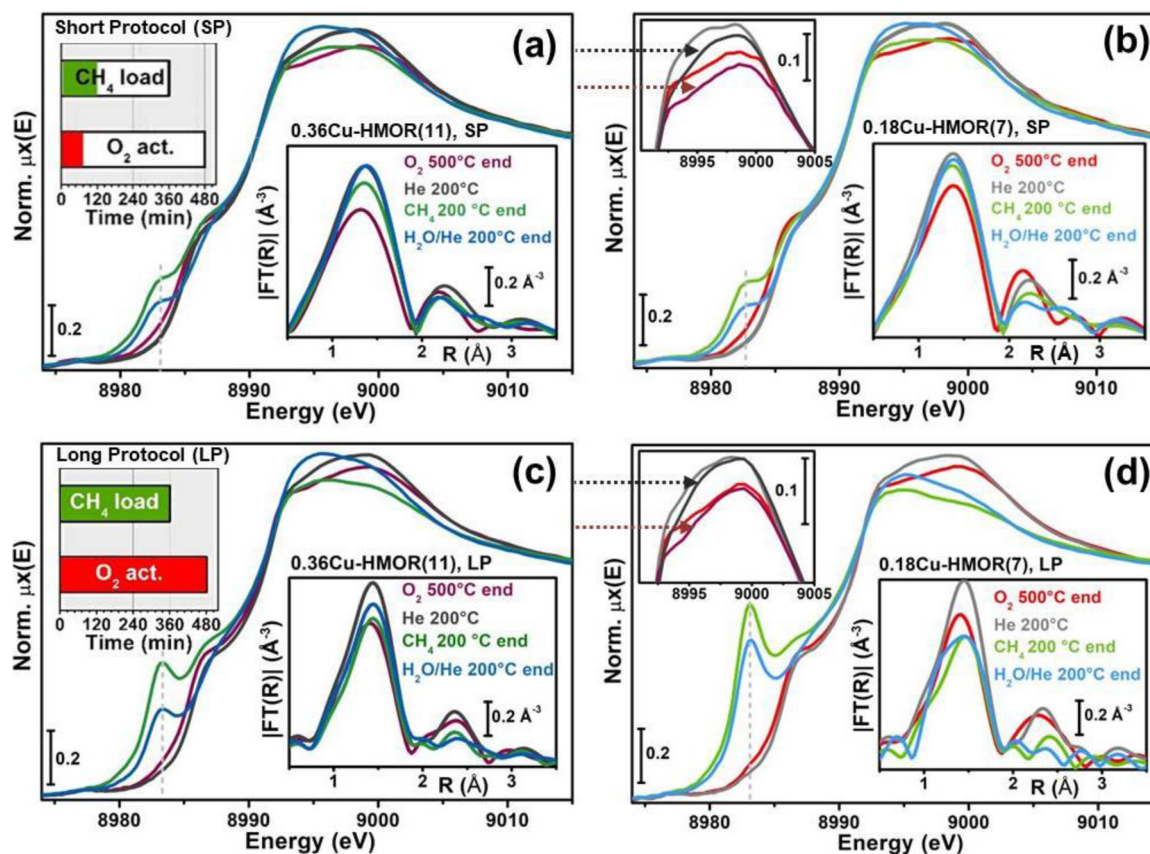
Each experimental XANES, μ^{EXP} (E), was fitted as a linear combination of the three reference XANES spectra, μ_i^{REF} (E), *i.e.*: μ^{LCF} (E) = $\Sigma_i w_i \, \mu_i^{REF}$ (E), optimizing the weights w_i for each reference spectrum. LCF was performed by setting the total sum of the weights to unity, $\Sigma_i w_i = 1$. For each analysed scan, the corresponding LCF R-factor was computed as

$$[\Sigma_j \, [\mu^{EXP}_j \, (E) - \mu^{LCF}_j \, (E)]^2 / \Sigma_j \, [\mu^{EXP}_j \, (E)]^2$$

where j denotes each experimental point in fitted energy range, (8970–9020) eV; R-factor = 0 corresponds to the ideal reproduction of the experimental curve: μ^{EXP} (E) $\equiv \mu^{LCF}$ (E).

2.4. Productivity evaluation by fixed-bed reactor laboratory tests

We employed laboratory bench reactor tests in order to evaluate the normalized CH_3OH productivity for the two materials under the same LP and SP conditions adopted in the *operando* XAS experiments (Fig. 1). The investigated Cu-zeolites were tested for the stepwise DMTM conversion in a quartz plug flow reactor of 6 mm internal diameter, using 100 mg of pelletized samples (425–250 μm). The reactor was heated by a tubular oven, with a thermocouple inserted in a capillary quartz tube in the middle of the sample bed for temperature control. Total flow rate

Fig. 2. On-line MS data for CH_3OH, CH_3OCH_3 (resulting from the condensation of two CH_3OH molecules), and H_2O, simultaneously collected along steam-assisted CH_3OH extraction during *operando* XAS at the BM23 beamline, following the LP for DMTM over (a) 0.36Cu-HMOR(11) and (b) 0.18Cu-HMOR(7).

Fig. 3. (a, b) Cu K-edge XANES spectra for (a) 0.36Cu-HMOR(11) and (b) 0.18Cu-HMOR(7) at key steps during the DMTM process carried out under the SP conditions. The inset of part (a) summarizes the duration of O_2-activation and CH_4-loading steps in the SP; the inset of part (b) compares the XANES spectra of the two materials after 90 min in O_2 at 500 °C, after cooling down to 200 °C and flushing the system with He in the white-line region. (c, d) As parts (a, b) but under the LP conditions. In all the panels, the bottom insets report the FT-EXAFS spectra corresponding to the XANES ones reported in the main panels, using the same colour code. FT-EXAFS were obtained by Fourier transforming the $k^2\chi(k)$ spectra in the (2.4–8.7) Å^{-1} range for SP experiments (parts a, b) and (2.4–11.0) Å^{-1} range for LP experiments (parts c, d); due to the different FT k-ranges, only a qualitative comparison between the EXAFS spectra collected under LP and SP conditions is possible. The characteristic XANES peak at ca. 8282.5 eV assigned to 1s → 4p transition in Cu(I) species is highlighted by dashed grey vertical bars (For interpretation of the references to colour in this figure legend, the reader is referred to the web version of this article).

for all the DMTM steps was 15 ml/min. The quantification of the products was performed online during steam-assisted extraction with a Hewlett Packard 6890/5972 GCMS.

3. Results and discussion

3.1. Operando XAS at key process steps: an overview on the impact of conditions and composition

We first focus on a comparative overview of the *operando* XAS spectra collected at the key steps of the DMTM conversion process for the four combinations of composition/conditions (Fig. 3). These are obtained by monitoring 0.18Cu-HMOR(7) and 0.36Cu-HMOR(11) materials during the applied reaction protocols, different in the duration of O_2-activation and CH_4-loading steps (see insets of Fig. 3a,c and Section 2.2 for details). Under both conditions 0.18Cu-HMOR(7) significantly outperforms 0.36Cu-HMOR(11): it produces 0.11 or 0.47 mol $CH_3OH/$ mol Cu at the SP and LP conditions, respectively, *vs* 0.07 or 0.25 mol $CH_3OH/$mol Cu for 0.36Cu-HMOR(11), as summarized in Table 2 (values from laboratory tests using the same fixed bed reactor and testing rig).

Table 2 also reports the mol $CH_3OH/$mol Cu evaluated from on-line MS data during *operando* XAS under the SP conditions. For consistency, in subsequent analyses we used for both LP and SP the laboratory data obtained with the same reactor and test rig. Nonetheless, the performance evaluated from on-line MS is in good agreement with laboratory

Table 2

Summary of the DMTM performance for the two Cu-MOR samples (mol CH_3OH /mol Cu), evaluated under the SP and LP conditions in the same fixed-bed reactor ('lab.' labels). For the SP protocol, the values obtained from MS data collected during operando XAS ('*operando*' label) are also reported for comparison.

Sample	Norm. productivity (mol $CH_3OH/$mol Cu)		
	SP, lab.	SP, *operando*	LP, lab.
0.36Cu-HMOR(11)	0.07 ± 0.01	0.08 ± 0.02	0.25 ± 0.03
0.18Cu-HMOR(7)	0.11 ± 0.01	0.13 ± 0.03	0.47 ± 0.06

results. This comparison corroborates the validity of correlations between the XAS results and the normalized productivity assessed into independent laboratory tests.

Fig. 3 shows the spectra collected at 500 °C in O_2 at the end of O_2-activation step, as well as after the samples have been cooled to 200 °C in O_2 and flushed with He, prior to interaction with CH_4. Scans collected at the end of the CH_4-loading step (120 or 360 min for SP and LP, respectively) and steam-assisted CH_3OH extraction (60 min in both protocols) are also reported.

In agreement with the abundant XAS literature on Cu-zeolites [11,12,28,36–40], O_2-activation at 500 °C in all cases results in a largely dominant Cu(II) oxidation state. The observed XAS features are consistent with tridentate O-ligated Cu(II) units, located at well-defined

ion-exchange sites in the zeolite framework. A well-defined second-shell peak stemming from Cu-Al/Si and Cu-Cu (for multi-copper species) scattering is also evident in the EXAFS of the two samples at the end of O_2-activation (bottom insets in Fig. 3).

Only subtle modifications are observed in the XAS spectra at the end of the O_2-activaton step, as a function of both the compositional and process parameters (red and purple curves in Fig. 3). Nonetheless, it is clear that certain differences exist, especially in the XANES white line (WL) region (see insets of Fig. 3b,d). During both SP and LP protocols, 0.18Cu-HMOR(7) shows a higher WL intensity, pointing to an higher first-shell coordination number.

Advanced experimental and analytical approaches would be required to discriminate the XAS signatures of different Cu(II) species co-existing in Cu-MOR after O_2-activation. The data reported here indicate that conventional XAS can detect minor modifications but is not sensitive enough for a quantitative assessment of Cu(II) speciation following high-temperature O_2-activation. With this respect, high energy-resolution X-ray spectroscopy at an undulator source [41,42], aided by statistical analysis and multivariate curve resolution [43,44] has proven to be a viable approach [16], in combination with site-selective spectroscopies (*e.g.* UV–vis and r-Raman [27,45,46]).

Nonetheless, it is interesting to note that longer O_2-activation time during LP, diminishes the gap in the WL intensity between 0.18Cu-HMOR(7) and 0.36Cu-HMOR(11). This observation is consistent with slow re-organization of Cu-species during the high-temperature O_2-activation step, progressively converting inactive Cu-species into active ones. These processes are expected to have only a minor impact on the average XAS signal, due to the similarity in the XAS signatures of the involved Cu(II) species. Conversely, they have a drastic impact on the material productivity as demonstrated by a more than triple CH_3OH productivity per mol Cu under LP conditions with respect to the SP ones for both samples (see Table 2).

Furthermore, XAS indicates changes in the coordination of Cu ions while the materials are cooled to 200 °C in O_2 and flushed with He prior to CH_4-loading (grey curves in Fig. 3). Indications are an additional increase of the WL in the XANES and of the first-shell peak in the EXAFS spectra beyond the expected decrease in the thermal contributions to the Debye-Waller factors from 500 °C to 200 °C. The exact origin of these modifications, also detected in Cu-CHA [12], is still to be clarified. Possible mechanisms could involve thermal-induced modification in the coordination mode of O_2 in Cu(II)/activated-O_2 complexes (typically, an end-on to side-on coordination swap), as well as a reduced mobility of the cations [47] as a consequence of the lower operation temperature. Both translate in a more uniform coordination environment over macroscopic sampling time.

The pronounced modifications occurring in the XAS during the CH_4-loading and steam-assisted CH_3OH extraction step, reflecting Cu(II) to Cu(I) reduction and subsequent hydration phenomena, greatly facilitate the identification of the different Cu species present, as well as the quantitative determination of their concentration profiles during the experiments.

From the overview reported in Fig. 3, it is clear that, in all the cases, Cu(I) species are formed during CH_4-loading at 200 °C (green curves). This is evidenced by the development of a rising-edge peak at ca. 8983 eV, assigned to 1s → 4p transitions in Cu(I) centres and is consistent with previous studies on Cu-zeolites [48–50] and, in particular, on Cu-MOR [11,13,28,38,44]. Importantly, while the energy position of the Cu(I) peak (together with the overall spectral shape) is conserved throughout the four experiments, its intensity shows important variations as a function of composition and reaction protocol. These evidences indicate that, most likely, the same Cu(I) species are formed irrespectively of the compositional/process parameters. However, the process parameters varied in the protocols drastically alter the Cu(I) concentration in the materials, in the same way as they do for the CH_3OH productivity per Cu.

Combining the most favourable compositional characteristics of

0.18Cu-HMOR(7) with the LP protocol (Fig. 3d), a very well developed Cu(I) state is observed after 360 min in CH_4 at 200 °C. This is a highly desirable condition for an absorbing-atom-averaged technique such as XAS to reliably assess the chemical nature of the Cu(I) moieties formed in parallel to the activation of CH_4. In particular, both the characteristic features in the XANES and the erosion of the second-shell peak in the EXAFS point to a quasi-linear, isolated Cu(I) site. At the end of steam-assisted extraction, the presence of hydrated Cu(II) ions is always observed and corroborated by the almost complete lack of the second-shell peak in the EXAFS. These modifications are accompanied by an apparent decrease of the normalized XANES intensity at the energy position of the Cu(I) fingerprint peak.

Further insights in the redox and structural dynamics involving Cu-ions during the CH_4-loading and the steam-assisted extraction steps will be presented in the following section by applying LCF analysis to time-resolved XANES collected under the SP and LP protocols.

### 3.2. Cu redox dynamics during CH_4-loading and steam-assisted CH_3OH extraction

Fig. 4 shows the time evolution of the Cu K-edge XANES spectra for the four combinations of compositions/protocols (SP, LP) explored in this study during the CH_4-loading and steam-assisted CH_3OH extraction steps, collected isothermally at 200 °C.

The progressive development of the characteristic Cu(I) peak at ca. 8983 eV as a function of the interaction time with CH_4 (green curves in Fig. 4) can be appreciated in the different time-frames adopted for *operando* XAS experiments using the SP (Fig. 4a,b) and the LP (Fig. 4c,d) protocol. Simultaneously, the WL intensity diminishes, in agreement with an average decrease in the first-shell coordination number of Cu ions (conversion of three-fold coordinated Cu(II) into two-fold coordinated Cu(I), consistent with the EXAFS results in Fig. 3). Once steam is admitted to the reactor, the XANES is promptly perturbed (blue curves in Fig. 4). A higher WL feature, peaking at ca. 8985 eV and a smoother rising-edge region are characteristic for the conversion of under-coordinated framework-interacting Cu(II) species into pseudo-octahedral Cu(II) aquo-complexes, highly mobile within the zeolite pores.

We have applied LCF analysis to evaluate the time-dependent concentration profiles of the different Cu-species simultaneously contributing to the *operando* XANES dataset in Fig. 4. This method has been largely employed in recent studies to monitor redox processes in Cu-based catalysts [12,13,28,51–55]. Although the simple LCF approach is unviable to distinguish between the Cu(II)-oxo moieties formed after O_2-activation, it has provided reliable results in the analysis of Cu-speciation during CH_4 activation at Cu active sites and subsequent steam-assisted CH_3OH extraction [12,28].

Fig. 5a reports the three reference XANES spectra used for LCF analysis (see also Section 2.3 for details). They are representative of solution-like Cu(II) aquo complexes (*Cu(II)-hyd,* blue curve in Fig. 5a); composition/protocol-specific framework-interacting Cu(II) species present in the system before interaction with CH_4 (*Cu(II)-MOR,* black curve in Fig. 5a) and Cu(I) species stabilized on the MOR zeolite (*Cu(I)-MOR,* red curve in Fig. 5a). The validity of the applied three-component LCF model is exemplified in Fig. 5b,c, comparing two representative experimental scans with their corresponding LCF best-fit curves and LCF residuals.

The quasi-linear nature of the *Cu(I)-MOR* state is demonstrated by the peculiarly high intensity of the Cu(I) 1s → 4p peak [56,57] as well as by the similarity with the XANES of the $[Cu(I)(NH_3)_2]^+$ linear complex [53,58–60] (reported in Fig. 5a for comparison). Interestingly, a preference for quasi-linear coordination (O_{fw}-Cu(I)-O_{fw} bond angles around 150°, where O_{fw} indicate O atoms of the zeolite framework) has been predicted from DFT for Cu(I) ions in the 10-member ring of ZSM-5 [61], and later extended to the coordination motif of Cu(I) in the 8-member side-pocket window in MOR [45]. DFT-assisted EXAFS analysis

ARTICLE IN PRESS

K.A. Lomachenko, et al.   Catalysis Today xxx (xxxx) xxx–xxx
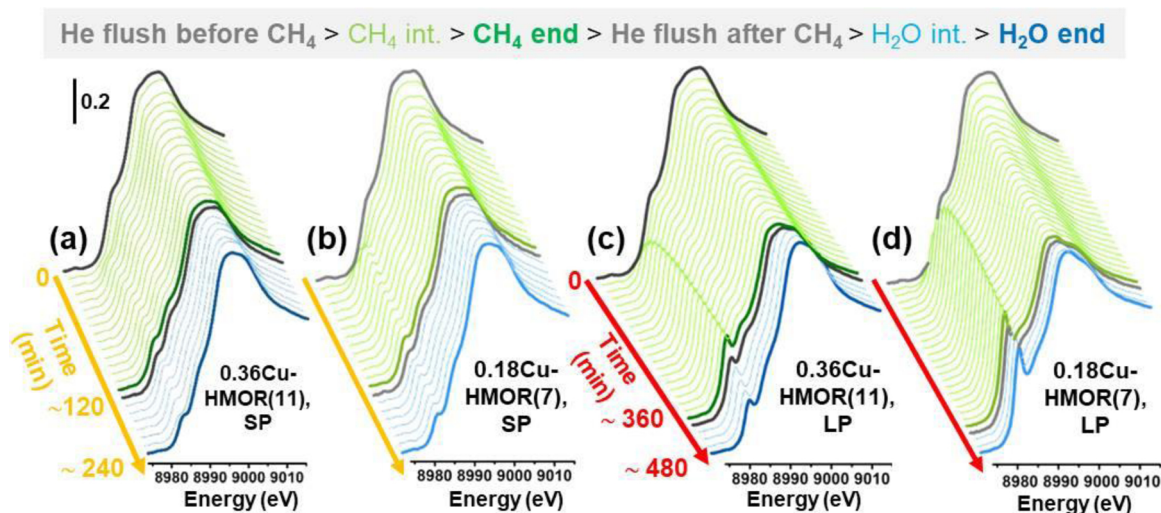
Fig. 4. Time-resolved Cu K-edge XANES spectra collected during the CH$_4$-loading and the steam-assisted CH$_3$OH extraction steps over two Cu-MOR samples under the SP and the LP conditions. (a) 0.36Cu-HMOR(11) and (b) 0.18Cu-HMOR(7) under the SP conditions, ca. 2 min/scan; (c) 0.36Cu-HMOR(11) and (d) 0.18Cu-HMOR (7) under the LP conditions, ca. 15 min/scan. For each sequence, the first spectrum reported in grey is collected at 200 °C in He flow, after O$_2$-activation and just before starting the CH$_4$-loading step, while the second one corresponds to the He flush separating the CH$_4$-loading (green curves) and the extraction (blue curves) steps (For interpretation of the references to colour in this figure legend, the reader is referred to the web version of this article).

of the *Cu(I)-MOR* state reported in Fig. 5a has recently supported the presence of such quasi-linear Cu(I) species in vacuum-activated Cu-MOR [62].

Fig. 6 summarizes the LCF results, reporting the concentration profiles for the three kinds of Cu-species included in our model as a function of the experiment time during CH$_4$-loading (green areas), He flush (grey areas), and steam-assisted extraction (blue areas). LCF R-factor values (also plotted in Fig. 6) are always below 4×10^{-4} and thus corroborate the validity of the adopted analysis approach.

The qualitative considerations presented above on the impact of composition and process steps duration on the reactivity are fully confirmed by the quantitative LCF results. In particular, a higher fraction of Cu(I) is formed during interaction with CH$_4$ under LP conditions at the expense of the *Cu(II)-MOR* component. The concentration of *Cu (I)-MOR* peaks to 42% and 66% of total Cu content, for 0.36Cu-HMOR (11) and 0.18Cu-HMOR, respectively, whereas it decreases to 22% and 30% if the SP is employed over the same two materials. From these values, it is clear that the compositional characteristics of 0.18Cu-HMOR(7) which promote the highest productivity per Cu, equally favour a more pronounced Cu(I) development during CH$_4$ activation.

Notably, the LCF analysis of the available time-resolved data allows

to monitor the dynamics of the Cu(II) to Cu(I) reduction process. The time-dependent concentration profiles for *Cu(I)-MOR* in Fig. 6 evidence how the maximum Cu(I) development occurs relatively early during the CH$_4$-loading step and is reached earlier for 0.18Cu-HMOR(7). Then the concentration of *Cu(I)-MOR* stabilizes indicating a saturation of the active Cu-sites formed during the O$_2$-activation step, to a much larger extent under the LP conditions. Once maximum Cu(I) development is reached, a slight decrease of Cu(I) fraction with time can be appreciated, counterbalanced by an increment in the fraction of *Cu(II)-MOR*. This effect becomes more pronounced once CH$_4$ is removed from the gas feed and the system is flushed with He prior to steam admission. The observed growth of Cu(I) can be safely connected with the molecular events yielding CH$_4$ activation at a Cu-site. However, it is still unclear how stable is the thus formed Cu(I) and how it interacts within the reaction environment. With this respect, Cu(I) disproportionation to Cu(0) and Cu(II) species can be excluded based on the absence of any trace of Cu(0) in the XANES. During the CH$_4$-loading step, LCF also indicates minor fractions (< 10% total Cu) of *Cu(II)-hyd*, similarly to what was observed in previous studies for both Cu-MOR and Cu-CHA [12,28]. This suggests that during interaction of the O$_2$-activated material with CH$_4$ (with possible overoxidation of the latter), small
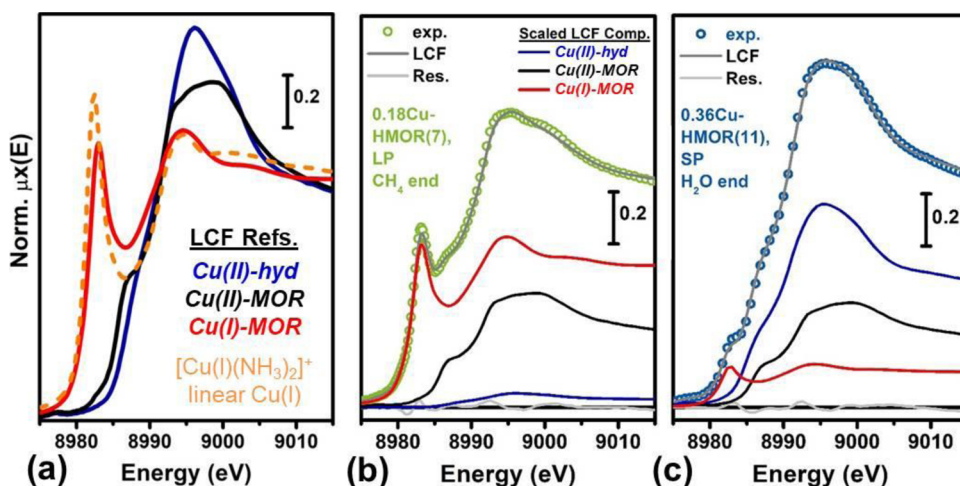
Fig. 5. (a) Reference XANES spectra employed for LCF analysis of the time-dependent XANES data, comprising hydrated Cu(II) aquo-complexes (blue); framework-coordinated Cu(II) species present at 200 °C after O$_2$-activation (black); Cu(I) species (red); [Cu(I)(NH$_3$)$_2$]$^+$ linear complex (dashed orange line, reported for comparison). (b) Example of LCF quality obtained for the *operando* XAS spectrum of Cu-MOR during the CH$_4$-loading. (c) Same as (b) for steam-assisted extraction step of the DMTM process. For each selected example, the figures report the experimental spectrum (coloured circles) in comparison with its best-fit curve (grey line), the scaled components, using the same colour code as in part (a), and the LCF residuals (light grey curves at the bottom of the plots) (For interpretation of the references to colour in this figure legend, the reader is referred to the web version of this article).
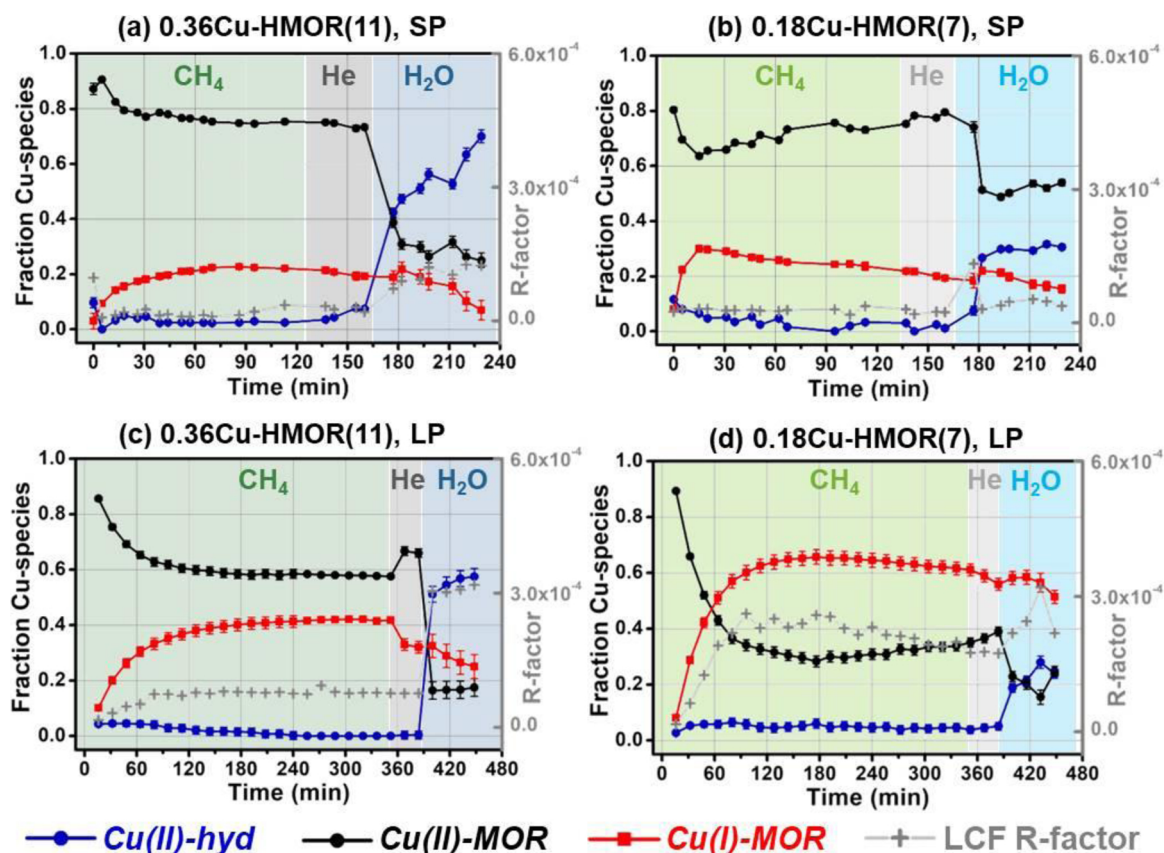
Fig. 6. Time-dependent concentration profiles of different Cu-species during CH_4-loading and extraction steps (reported as fraction of total Cu, left ordinate axis) evaluated from XANES LCF analysis for the four combinations of composition/reaction protocol investigated in this work: (a) SP over 0.36Cu-HMOR(11); (b) SP over 0.18Cu-HMOR(7); (c) LP over 0.36Cu-HMOR(11); (d) LP over 0.18Cu-HMOR(7). The LCF R-factor is reported in each panel (grey symbols, right ordinate axis). In some case the statistical error bars are smaller than the adopted symbol size (For interpretation of the references to colour in this figure legend, the reader is referred to the web version of this article).

quantities of H_2O might be produced, which might slowly interact with the *Cu(I)-MOR* species present in the system.

Not surprisingly, the concentration of *Cu(II)-hyd* abruptly increases as soon as steam is introduced. Importantly, the initial growth step in the fraction of *Cu(II)-hyd* is mirrored by a negative step in the concentration of *Cu(II)-MOR*. This indicates that, once steam is admitted to the sample at 200 °C, some *Cu(II)-MOR* species are prone to be immediately hydrolysed. The time evolution of the *Cu(I)-MOR* component monitored during extraction is completely different. In qualitative agreement with the results by Sushkevich et al. [13], it undergoes a slow and gradual decrease with time, resulting after 60 min of extraction in the loss of ca. 20% (LP) and 60% (SP) of the Cu(I) present before H_2O admission in 0.36Cu-HMOR(11) and of ca. 10% (LP) and 20% (SP) in 0.18Cu-HMOR(7).

3.3. Mechanistic insights from operando XAS

The fractional contributions from the different types of Cu species estimated by XANES LCF can quantitatively be correlated to the CH_3OH productivity. Crucially, these have to be evaluated under the same reaction conditions if quantitative relationships between Cu-speciation and activity are to be obtained. To this aim, we have plotted in Fig. 7a the mol CH_3OH/mol Cu *vs* the maximum Cu(I) fraction detected during the CH_4-loading step for each of the four composition/protocol combinations examined in this study (points A–D in Fig. 7a).

The four experimental points indicate a positive linear correlation between the normalized productivity and the relative abundance of *Cu(I)-MOR* species formed during CH_4-loading, best-fitted by a y [mol CH_3OH/mol Cu] = (0.9 ± 0.1) x [mol Cu(I)/mol Cu] – (0.14 ± 0.03)

trend-line. The linear fit provides a very good model to describe our experimental observations, resulting in an adjusted $R^2 = 0.953$. Thus, the fraction of Cu(I) formed when the O_2-activated material is exposed to CH_4 is demonstrated to be a good, spectroscopically accessible, descriptor of the CH_3OH productivity per Cu. This general result is in agreement with the recent work by Newton et al. [30], where, on the basis of own and literature data for different Cu-zeolites evaluated under both high-temperature and isothermal/high-pressure approaches to DMTM, the authors also correlate the XANES-derived fraction of Cu (I) and the methanol productivity assessed in independent laboratory tests.

Some considerations on the best-fit line in Fig. 7a can provide preliminary insights on the DMTM reaction mechanism over the investigated Cu-MOR materials. The obtained slope of (0.9 ± 0.1) – very close to unity – suggests that for a single CH_3OH molecule produced in the DMTM process over the investigated materials, one Cu ion gets reduced to Cu(I). Assuming a mono(μ-oxo) dicopper(II) active site [12,13,16,28,45], this observation suggests a mixed-valence Cu(II)/Cu (I) configuration upon (μ-O) methylation, such as in **Z**[Cu(I)(OCH$_3$)Cu (II)]**Z** (where **Z** denotes coordination to two zeolite framework oxygen atoms O_{fw} in the proximity of a charge-balancing Al at a T-site). Furthermore, the best-fit line has a negative intercept of – 0.14 mol CH_3OH/mol Cu. This translates in a ca. 15% Cu(I)/total Cu offset detected in correspondence of a null CH_3OH productivity (orange arrow in Fig. 7a). This offset could be connected with (i) CO_x species extracted during steam-assisted extraction as CH_3OH overoxidation products (setting the selectivity in the 80–90% range) and (ii) direct oxidation of CH_4 to CO and CO_2 during CH_4-loading, both producing a Cu(I) ion without contributing to the CH_3OH yield per Cu considered in our
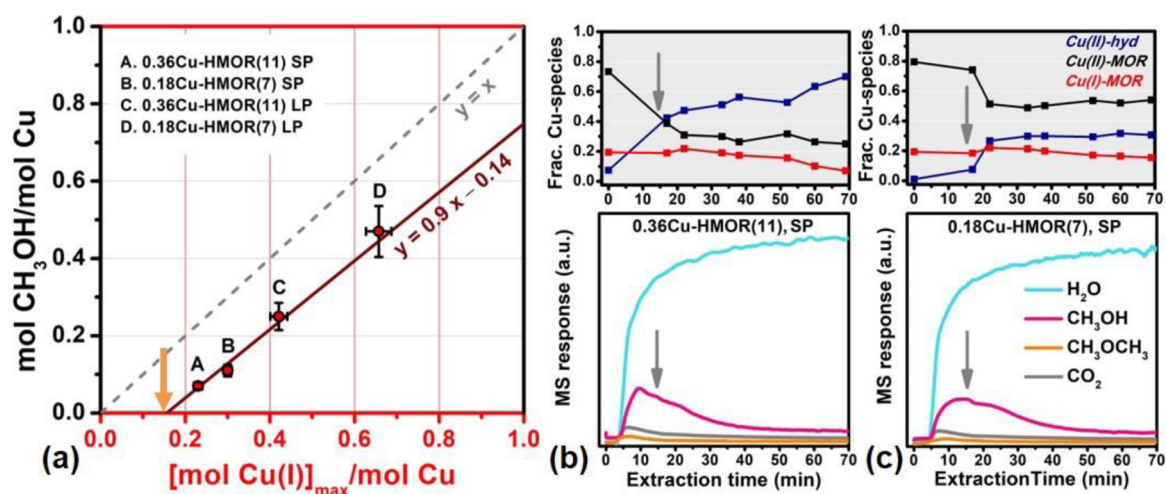
Fig. 7. (a) Correlation between the maximum fraction of Cu(I) detected by XAS during the CH_4-loading step and the CH_3OH productivity per Cu for the four combinations of compositions/protocols explored in this work. For consistency, for all the experimental points, the CH_3OH productivity per Cu is obtained from laboratory tests in the same fixed-bed reactor under the same conditions as *operando* XAS experiments (see Table 2, 'lab.' values). (b, c) Comparison between Cu-speciation from XANES LCF at the SP conditions (top panels) and on-line MS profiles for H_2O, CH_3OH, CH_3OCH_3 (resulting from the condensation of two CH_3OH molecules) and CO_2 simultaneously collected along steam-assisted CH_3OH extraction during *operando* XAS (bottom panels), for (b) 0.36Cu-HMOR(11) and (c) 0.18Cu-HMOR(7). The grey arrows mark the peak in CH_3OH release (For interpretation of the references to colour in this figure legend, the reader is referred to the web version of this article).

correlation.

The formation of Cu(I) during the CH_4-loading step is well documented in the literature on DMTM over Cu-zeolites [11–13,28,30]. However, in most cases, a limited development of Cu(I) (typically up to ca. 30% total Cu) is observed in the XANES. Consistently, only minor modifications are detected in the EXAFS, leading to the working hypothesis of a substantial conservation of the di-copper active-site structure during CH_4 activation and stabilization of methyl groups. This appears in contrast with the XAS results obtained here under conditions allowing an optimal development of Cu(I), as well as a higher CH_3OH productivity per Cu. The typical XANES fingerprints of a quasi-linear two-fold coordinated Cu(I) (see Fig. 5a,b) and the pronounced erosion of the second-shell peak in the EXAFS (see bottom inset of Fig. 3d) both support opening of the Cu-(μ-O)-Cu bridge in mono(μ-oxo) dicopper cores upon (μ-O) methylation, together with important rearrangements in the coordination of the Cu(I) ion to the framework. A possible scenario could involve the di-copper core dissociation into proximal Cu(I)/Cu(II) units, *e.g.* a bare **Z**Cu(I) ion and a methoxide **Z**[Cu(II)(OCH₃)] complex.

Additional indications can be obtained by matching the XANES LCF results during steam-assisted extraction with the corresponding on-line MS profiles, here obtained with suitable quality under the SP conditions (Fig. 7b,c). The presence of two distinct processes triggered by H_2O during the extraction step has been already discussed in Section 3.2. These include: (i) a quick hydrolysis of *Cu(II)-MOR* species to *Cu(II)-hyd.* ones (occurring within 20 min of extraction in both the investigated samples, see top panels in Fig. 7b,c); (ii) a gradual diminution of the *Cu(I)-MOR* contribution, becoming appreciable only after 40 min of extraction at the SP conditions. The MS peak corresponding to CH_3OH release is synchronized with the first process, as highlighted by vertical grey arrows in Fig. 7b,c. These results suggest that the adsorbed intermediates formed during CH_4-loading are released and converted to CH_3OH during the hydrolysis of a Cu(II) species, such as the **Z**[Cu(II)(OCH₃)] complexes mentioned before, rather than in connection with the H_2O-mediated re-oxidation pathways yielding the slow decay of the Cu(I) component.

Taken together, *operando* XANES, EXAFS and on-line mass spectrometry are able to provide significant mechanistic insights into the stoichiometric DMTM reaction over Cu-MOR, to be further deepened in

future experiments and validated against computational analysis.

4. Conclusions

In this work we have applied *operando* XAS to shed light on the stepwise DMTM conversion over Cu-MOR zeolites. We have explored in detail the influence of the reaction conditions (short *vs* long protocols) for two Cu-MOR materials yielding a markedly different performance in DMTM (roughly, a factor of two in normalized CH_3OH yield, if tested under the same conditions). While the duration of O_2-activation and CH_4-loading steps is known to drastically impact the CH_3OH productivity, we have provided here direct evidence of how these process parameters drive Cu-speciation along the reaction cycle.

Subtle differences in the XANES and EXAFS spectra of the two materials after O_2-activation indicate coexistence of both active and inactive Cu(II) species. XAS also supports rearrangement of the local coordination environment and siting of framework-coordinated Cu(II) ions during prolonged oxidizing treatment at 500 °C, as well as during the subsequent cooling step to 200 °C. Much more pronounced modifications are observed during the CH_4-loading step and subsequent steam-assisted CH_3OH extraction, facilitating the quantitative evaluation of Cu-speciation from *operando* XAS. With this respect, LCF analysis of time-dependent XANES has allowed us to discriminate among the different Cu-species present in the reaction mixture, as well as to quantify their concentration profiles. The CH_3OH yield per Cu (evaluated at the same conditions as used for XAS) and the maximum concentration of Cu(I) formed during the CH_4-loading step show a direct linear correlation, with a slope compatible with unity (mol CH_3OH extracted/mol Cu(I) formed during CH_4 activation ~ 0.9). Notably, the linear relation between the two materials' Cu(I) contents is independent of the applied reaction protocol (SP and LP). It also accurately models experimental data obtained using different setups (capillary with powder *vs* reactor cell with self-supporting pellet - shown to mutually possess both *pros* and *cons* when employed to study the DMTM reaction over Cu-zeolites).

The fraction of Cu(I) formed when the O_2-activated material is exposed to CH_4 is proven to represent a spectroscopically-accessible descriptor of the CH_3OH productivity per Cu. Under the most favourable compositional and process parameters (0.18Cu-HMOR(7), LP), we

ARTICLE IN PRESS

detect up to 66% of Cu occurring as quasi-linear Cu(I) species. The correspondent EXAFS spectrum indicates important modifications in the Cu active-site structure upon CH_4 activation and stabilization of reactive intermediates. A direct comparison between on-line MS data and XANES LCF results during steam-assisted extraction suggests that CH_3OH stems from the hydrolysis of a Cu(II)-methoxide adduct rather than from the decay of the Cu(I) component, evolving on a slower time-scale.

On the methodological ground, this work underlines how it is possible to establish quantitative correlations by adopting the same DMTM reaction conditions for both spectroscopy and productivity evaluation. With this respect, the time limitations generally associated with synchrotron experiments appear in conflict with the prolonged interaction times required to boost DMTM productivity. Nonetheless, the results obtained here demonstrate how certain Cu-speciation-activity relationships are conserved under different reaction protocols, over a wide productivity range. While LP conditions ensure a 'cleaner' spectroscopic response, shorter experiments can still provide valuable information, as long as the productivity is evaluated under the same protocols. The spectroscopic and mechanistic insights reported here contribute to advance in the fundamental understanding of DMTM conversion over Cu-MOR and, more generally, of redox chemistry in Cu-exchanged zeolites.

Acknowledgments

References

[1] G.A. Olah, A. Goeppert, M. Czaun, T. Mathew, R.B. May, G.K. Prakash, J. Am. Chem. Soc. 137 (2015) 8720–8729.
[2] C. Elvidge, M. Zhizhin, K. Baugh, F.-C. Hsu, T. Ghosh, Energies 9 (2016) 14.
[3] J.R. Rostrup-Nielsen, Catal. Today 21 (1994) 257–267.
[4] V. Arutyunov, Chapter 8 - direct methane to methanol: promising technologies based on the DMTM process, in: A. Basile, F. Dalena (Eds.), Methanol, Elsevier, 2018, pp. 211–238.
[5] J.H. Lunsford, Catal. Today 63 (2000) 165–174.
[6] D. Saha, H.A. Grappe, A. Chakraborty, G. Orkoulas, Chem. Rev. 116 (2016) 11436–11499.
[7] M. Ravi, M. Ranocchiari, J.A. van Bokhoven, Angew. Chem. Int. Ed. 56 (2017) 16464–16483.
[8] P. Tomkins, A. Mansouri, S.E. Bozbag, F. Krumeich, M.B. Park, E.M. Alayon, M. Ranocchiari, J.A. van Bokhoven, Angew. Chem. Int. Ed. 55 (2016) 5467–5471.
[9] M.H. Groothaert, P.J. Smeets, B.F. Sels, P.A. Jacobs, R.A. Schoonheydt, J. Am. Chem. Soc. 127 (2005) 1394–1395.
[10] E.M. Alayon, M. Nachtegaal, M. Ranocchiari, J.A. van Bokhoven, Chem. Commun. 48 (2012) 404–406.
[11] S. Grundner, M.A. Markovits, G. Li, M. Tromp, E.A. Pidko, E.J. Hensen, A. Jentys, M. Sanchez-Sanchez, J.A. Lercher, Nat. Commun. 6 (2015) 7546.
[12] D.K. Pappas, E. Borfecchia, M. Dyballa, I.A. Pankin, K.A. Lomachenko, A. Martini, M. Signorile, S. Teketel, B. Arstad, G. Berlier, C. Lamberti, S. Bordiga, U. Olsbye, K.P. Lillerud, S. Svelle, P. Beato, J. Am. Chem. Soc. 139 (2017) 14961–14975.
[13] V.L. Sushkevich, D. Palagin, M. Ranocchiari, J.A. van Bokhoven, Science 356 (2017) 523–527.
[14] P. Tomkins, M. Ranocchiari, J.A. van Bokhoven, Acc. Chem. Res. 50 (2017) 418–425.
[15] V.L. Sushkevich, D. Palagin, J.A. van Bokhoven, Angew. Chem. Int. Ed. 57 (2018) 8906–8910.
[16] D.K. Pappas, A. Martini, M. Dyballa, K. Kvande, S. Teketel, K.A. Lomachenko, R. Baran, P. Glatzel, B. Arstad, G. Berlier, C. Lamberti, S. Bordiga, U. Olsbye, S. Svelle, P. Beato, E. Borfecchia, J. Am. Chem. Soc. 140 (2018) 15270–15278.
[17] M. Dyballa, D.K. Pappas, K. Kvande, E. Borfecchia, B. Arstad, P. Beato, U. Olsbye, S. Svelle, ACS Catal. 9 (2019) 365–375.
[18] M.B. Park, S.H. Ahn, A. Mansouri, M. Ranocchiari, J.A. van Bokhoven, ChemCatChem 9 (2017) 3705–3713.
[19] A.J. Knorpp, A.B. Pinar, M.A. Newton, V.L. Sushkevich, J.A. van Bokhoven, ChemCatChem 10 (2018) 5593–5596.
[20] B. Ipek, M.J. Wulfers, H. Kim, F. Göltl, I. Hermans, J.P. Smith, K.S. Booksh, C.M. Brown, R.F. Lobo, ACS Catal. 7 (2017) 4291–4303.
[21] E. Borfecchia, D.K. Pappas, M. Dyballa, K.A. Lomachenko, C. Negri, M. Signorile, G. Berlier, Catal. Today (2018), https://doi.org/10.1016/j.cattod.2018.07.028 in press.
[22] E. Borfecchia, P. Beato, S. Svelle, U. Olsbye, C. Lamberti, S. Bordiga, Chem. Soc. Rev. 47 (2018) 8097–8133.
[23] D. Palagin, A.J. Knorpp, A.B. Pinar, M. Ranocchiari, J.A. van Bokhoven, Nanoscale 9 (2017) 1144–1153.
[24] K.D. Vogiatzis, G. Li, E.J.M. Hensen, L. Gagliardi, E.A. Pidko, J. Phys. Chem. C 121 (2017) 22295–22302.
[25] H.V. Le, S. Parishan, A. Sagaltchik, C. Göbel, C. Schlesiger, W. Malzer, A. Trunschke, R. Schomäcker, A. Thomas, ACS Catal. 7 (2017) 1403–1412.
[26] Y. Kim, T.Y. Kim, H. Lee, J. Yi, Chem. Commun. 53 (2017) 4116–4119.
[27] J.S. Woertink, P.J. Smeets, M.H. Groothaert, M.A. Vance, B.F. Sels, R.A. Schoonheydt, E.I. Solomon, Proc. Natl. Acad. Sci. U. S. A. 106 (2009) 18908–18913.
[28] E.M.C. Alayon, M. Nachtegaal, A. Bodi, J.A. van Bokhoven, ACS Catal. 4 (2014) 16–22.
[29] E.M.C. Alayon, M. Nachtegaal, E. Kleymenov, J.A. van Bokhoven, Microporous Mesoporous Mater. 166 (2013) 131–136.
[30] M.A. Newton, A.J. Knorpp, A.B. Pinar, V.L. Sushkevich, D. Palagin, J.A. van Bokhoven, J. Am. Chem. Soc. 140 (2018) 10090–10093.
[31] P.M. Abdala, O.V. Safonova, G. Wiker, W. van Beek, H. Emerich, J.A. van Bokhoven, J. Sa, J. Szlachetko, M. Nachtegaal, Chimia 66 (2012) 699–705.
[32] O. Mathon, A. Beteva, J. Borrel, D. Bugnazet, S. Gatla, R. Hino, I. Kantor, T. Mairs, M. Munoz, S. Pasternak, F. Perrin, S. Pascarelli, J. Synchrotron Radiat. 22 (2015) 1548–1554.
[33] G. Agostini, D. Meira, M. Monte, H. Vitoux, A. Iglesias-Juez, M. Fernandez-Garcia, O. Mathon, F. Meunier, G. Berruyer, F. Perrin, S. Pasternak, T. Mairs, S. Pascarelli, B. Gorges, J. Synchrotron Radiat. 25 (2018) 1745–1752.
[34] S. Bordiga, E. Groppo, G. Agostini, J.A. van Bokhoven, C. Lamberti, Chem. Rev. 113 (2013) 1736–1850.
[35] B. Ravel, M. Newville, J. Synchrotron Radiat. 12 (2005) 537–541.
[36] G. Turnes Palomino, P. Fisicaro, S. Bordiga, A. Zecchina, E. Giamello, C. Lamberti, J. Phys. Chem. B 104 (2000) 4064–4073.
[37] F.X. Llabrés i Xamena, P. Fisicaro, G. Berlier, A. Zecchina, G. Turnes Palomino, C. Prestipino, S. Bordiga, E. Giamello, C. Lamberti, J. Phys. Chem. B 107 (2003) 7036–7044.
[38] E. Borfecchia, K.A. Lomachenko, F. Giordanino, H. Falsig, P. Beato, A.V. Soldatov, S. Bordiga, C. Lamberti, Chem. Sci. 6 (2015) 548–563.
[39] E.M. Alayon, M. Nachtegaal, A. Bodi, M. Ranocchiari, J.A. van Bokhoven, Phys. Chem. Chem. Phys. 17 (2015) 7681–7693.
[40] C.W. Andersen, E. Borfecchia, M. Bremholm, M.R.V. Jorgensen, P.N.R. Vennestrom, C. Lamberti, L.F. Lundegaard, B.B. Iversen, Angew. Chem. Int. Ed. 56 (2017) 10367–10372.
[41] P. Glatzel, U. Bergmann, Coord. Chem. Rev. 249 (2005) 65–95.
[42] J. Singh, C. Lamberti, J.A. van Bokhoven, Chem. Soc. Rev. 39 (2010) 4754–4766.
[43] J. Jaumot, R. Gargallo, A. de Juan, R. Tauler, Chemometr. Intell. Lab. Syst. 76 (2005) 101–110.
[44] A. Martini, E. Borfecchia, K.A. Lomachenko, I.A. Pankin, C. Negri, G. Berlier, P. Beato, H. Falsig, S. Bordiga, C. Lamberti, Chem. Sci. 8 (2017) 6836–6851.
[45] P. Vanelderen, B.E. Snyder, M.L. Tsai, R.G. Hadt, J. Vancauwenbergh, O. Coussens, R.A. Schoonheydt, B.F. Sels, E.I. Solomon, J. Am. Chem. Soc. 137 (2015) 6383–6392.
[46] B.E.R. Snyder, M.L. Bols, R.A. Schoonheydt, B.F. Sels, E.I. Solomon, Chem. Rev. 118 (2018) 2718–2768.
[47] F. Göltl, P. Sautet, I. Hermans, Catal. Today 267 (2016) 41–46.
[48] C. Lamberti, S. Bordiga, M. Salvalaggio, G. Spoto, A. Zecchina, F. Geobaldo, G. Vlaic, M. Bellatreccia, J. Phys. Chem. B 101 (1997) 344–360.
[49] C. Lamberti, G. Turnes Palomino, S. Bordiga, G. Berlier, F. D'Acapito, A. Zecchina, Angew. Chem. Int. Ed. 39 (2000) 2138–2141.
[50] C. Prestipino, G. Berlier, F. Xamena, G. Spoto, S. Bordiga, A. Zecchina, G. Turnes Palomino, T. Yamamoto, C. Lamberti, Chem. Phys. Lett. 363 (2002) 389–396.
[51] C. Lamberti, C. Prestipino, F. Bonino, L. Capello, S. Bordiga, G. Spoto, A. Zecchina, S.D. Moreno, B. Cremaschi, M. Garilli, A. Marsella, D. Carmello, S. Vidotto, G. Leofanti, Angew. Chem. Int. Ed. 41 (2002) 2341–2344.
[52] N.B. Muddada, U. Olsbye, L. Caccialupi, F. Cavani, G. Leofanti, D. Gianolio, S. Bordiga, C. Lamberti, Phys. Chem. Chem. Phys. 12 (2010) 5605–5618.
[53] K.A. Lomachenko, E. Borfecchia, C. Negri, G. Berlier, C. Lamberti, P. Beato, H. Falsig, S. Bordiga, J. Am. Chem. Soc. 138 (2016) 12025–12028.
[54] C. Paolucci, I. Khurana, A.A. Parekh, S.C. Li, A.J. Shih, H. Li, J.R. Di Iorio, J.D. Albarracin-Caballero, A. Yezerets, J.T. Miller, W.N. Delgass, F.H. Ribeiro, W.F. Schneider, R. Gounder, Science 357 (2017) 898–903.
[55] A. Marberger, A.W. Petrov, P. Steiger, M. Elsener, O. Kröcher, M. Nachtegaal, D. Ferri, Nat. Catal. 1 (2018) 221–227.
[56] L.S. Kau, D.J. Spira-Solomon, J.E. Pennerhahn, K.O. Hodgson, E.I. Solomon, J. Am. Chem. Soc. 109 (1987) 6433–6442.
[57] E.I. Solomon, D.E. Heppner, E.M. Johnston, J.W. Ginsbach, J. Cirera, M. Qayyum,

M.T. Kieber-Emmons, C.H. Kjaergaard, R.G. Hadt, L. Tian, Chem. Rev. 114 (2014) 3659–3853.

[58] K. Mathisen, M. Stockenhuber, D.G. Nicholson, Phys. Chem. Chem. Phys. 11 (2009) 5476–5488.

[59] F. Giordanino, E. Borfecchia, K.A. Lomachenko, A. Lazzarini, G. Agostini, E. Gallo, A.V. Soldatov, P. Beato, S. Bordiga, C. Lamberti, J. Phys. Chem. Lett. 5 (2014) 1552–1559.

[60] T.V.W. Janssens, H. Falsig, L.F. Lundegaard, P.N.R. Vennestrøm, S.B. Rasmussen,

P.G. Moses, F. Giordanino, E. Borfecchia, K.A. Lomachenko, C. Lamberti, S. Bordiga, A. Godiksen, S. Mossin, P. Beato, ACS Catal. 5 (2015) 2832–2845.

[61] M.-L. Tsai, R.G. Hadt, P. Vanelderen, B.F. Sels, R.A. Schoonheydt, E.I. Solomon, J. Am. Chem. Soc. 136 (2014) 3522–3529.

[62] C. Buono, A. Martini, I.A. Pankin, D.K. Pappas, C. Negri, K. Kvande, K.A. Lomachenko, E. Borfecchia, Rad. Phys. Chem. (2018), https://doi.org/10.1016/j.radphyschem.2018.12.031 in press.